OPTICAL METAMATERIALS

Hierarchically porous polymer coatings for highly efficient passive daytime radiative cooling

Jyotirmoy Mandal[1], Yanke Fu[1], Adam C. Overvig[1], Mingxin Jia[2], Kerui Sun[1], Norman N. Shi[1], Hua Zhou[3,4], Xianghui Xiao[3,4], Nanfang Yu[1]*, Yuan Yang[1]*

Passive daytime radiative cooling (PDRC) involves spontaneously cooling a surface by reflecting sunlight and radiating heat to the cold outer space. Current PDRC designs are promising alternatives to electrical cooling but are either inefficient or have limited applicability. We present a simple, inexpensive, and scalable phase inversion–based method for fabricating hierarchically porous poly(vinylidene fluoride-co-hexafluoropropene) [P(VdF-HFP)$_{HP}$] coatings with excellent PDRC capability. High, substrate-independent hemispherical solar reflectances (0.96 ± 0.03) and long-wave infrared emittances (0.97 ± 0.02) allow for subambient temperature drops of ~6°C and cooling powers of ~96 watts per square meter (W m^{-2}) under solar intensities of 890 and 750 W m^{-2}, respectively. The performance equals or surpasses those of state-of-the-art PDRC designs, and the technique offers a paint-like simplicity.

Cooling human-made structures, such as buildings, is a widespread necessity faced by humans today (*1*). However, compression-based cooling systems that are prevalently used (e.g., air conditioners) consume substantial amounts of energy, have a net heating effect, require ready access to electricity, and often require coolants that are ozone-depleting or have a strong greenhouse effect (*2, 3*). Therefore, inexpensive, eco-friendly approaches with net cooling capability are desirable for reducing energy costs, operation time, and associated ozone-depleting and CO$_2$ emissions from traditional cooling systems, or providing relief where electrical cooling is not available. One alternative to energy-intensive cooling methods is passive daytime radiative cooling (PDRC)—a phenomenon where a surface spontaneously cools by reflecting sunlight [wavelengths (λ) ~0.3 to 2.5 µm] and radiating heat to the cold outer space through the atmosphere's long-wave infrared (LWIR) transmission window (λ ~ 8 to 13 µm). PDRC is most effective if a surface has a high, hemispherical solar reflectance ($\bar{R}_{solar}$) that minimizes solar heat gain and a high, hemispherical, LWIR thermal emittance ($\bar{\epsilon}_{LWIR}$) that maximizes radiative heat loss (*4*). If $\bar{R}_{solar}$ and $\bar{\epsilon}_{LWIR}$ are sufficiently high, a net radiative heat loss can occur, even under sunlight. The passive nature of this effect makes PDRC highly appealing, as cooling occurs without the need for electricity, refrigerants, or mechanical pumps that require maintenance.

Research in recent decades has yielded a variety of PDRC designs comprising sophisticated emissive coatings such as photonic structures, dielectrics, polymers, and polymer-dielectric composites on metal mirrors (*5–11*). Although efficient, these designs are costly and susceptible to corrosion. Furthermore, unlike paints, they are prefabricated and cannot be directly applied to existing roofs or walls, which have various compositions, textures, and geometries (*7, 9, 10*). Therefore, cool-roof paints (CRPs), which combine a modest optical performance with easy applicability and inexpensiveness, remain the benchmark for PDRC (*12–15*). However, CRPs, which consist of dielectric pigments (e.g., titania and zinc oxide) embedded in a polymer matrix, have a low solar reflectance (typically ~0.85) due to the pigments' ultraviolet (UV) absorptance and the low near-to-short–wavelength infrared (NIR-to-SWIR, λ ~0.7 to 2.5 µm) reflectance (*13*). We realized that replacing the pigments in CRPs with light-scattering air voids can not only eliminate this problem and increase the optical performance to state-of-the-art levels, but also avoid the material, processing, and environmental costs associated with pigments (*14, 16*). Inspired by this idea, we report a simple, scalable, and inexpensive phase inversion–based process for fabricating hierarchically porous polymer coatings that exhibit excellent $\bar{R}_{solar}$ and $\bar{\epsilon}_{LWIR}$. Specifically, we achieved substrate-independent hemispherical $\bar{R}_{solar}$ = 0.96 ± 0.03 and $\bar{\epsilon}_{LWIR}$ = 0.97 ± 0.02 with hierarchically porous poly(vinylidene fluoride-co-hexafluoropropene) [P(VdF-HFP)$_{HP}$]. The values result in a superb PDRC capability, exemplified by a subambient cooling of ~6°C and an average cooling power of ~96 W m^{-2} under solar intensities of 890 and 750 W m^{-2}, respectively. The performance is on par with or exceeds those in previous reports (*7, 9, 10*). Because the fabrication technique is room-temperature– and solution-based, the porous polymer coatings can be applied by conventional approaches like painting and spraying to diverse surfaces such as plastics,

metal, and wood. Moreover, it can incorporate dyes to achieve a desirable balance between color and cooling performance. The performance of the coatings and the paint-like convenience of the technique make it promising as a viable way to achieve high-performance PDRC.

Our phase inversion–based method for making hierarchically porous polymers starts with the preparation of a precursor solution of P(VdF-HFP) (polymer) and water (nonsolvent) in acetone (solvent) (Fig. 1A). We apply a film onto a substrate and dry it in air. The rapid evaporation of the volatile acetone causes the P(VdF-HFP) to phase-separate from the water, which forms micro- and nanodroplets. The P(VdF-HFP)$_{HP}$ coating is formed (Fig. 1, A and B) after the water evaporates. The micro- and nanopores in the coating efficiently backscatter sunlight and enhance thermal emittance (Fig. 1C). Consequently, P(VdF-HFP)$_{HP}$ films with ~50% porosity and thickness ≳300 µm have an exceptional, substrate-independent hemispherical $\bar{R}_{solar}$ of 0.96 and $\bar{\epsilon}_{LWIR}$ of 0.97 (Fig. 1, D to F). At thicknesses ≳500 µm, $\bar{R}_{solar}$ ≳0.98 is achieved (figs. S2 and S15). The high $\bar{R}_{solar}(\theta)$ ensures excellent reflection of sunlight from all incidences (Fig. 1E) and eliminates the need for silver reflectors used in previous designs (*7, 9, 10*), while the high $\bar{\epsilon}_{LWIR}(\theta)$ leads to a hemispherical $\bar{\epsilon}_{LWIR}$ that is >10% higher than previously reported values (Fig. 1F) (*7, 9*). The precursor's paint-like applicability makes P(VdF-HFP)$_{HP}$ attractive for practical use.

P(VdF-HFP) (Fig. 2A) has ideal intrinsic electromagnetic properties for PDRC applications. First, it has a negligible extinction coefficient across the solar wavelengths (λ = 0.3 to 2.5 µm) (Fig. 2B), unlike dielectric pigments of paints (fig. S10) and silver, which both absorb UV light. This keeps solar heating to a minimum. Second, the polymer has multiple extinction peaks in the thermal wavelengths, including 14 in the LWIR window, which arise from the different vibrational modes of its molecular structure (Fig. 2B) (*17–19*). Consequently, P(VdF-HFP) efficiently radiates heat in the LWIR window, where peak blackbody emissions from terrestrial surfaces and a high atmospheric transmittance into space coincide.

When structured by the phase-inversion technique into a hierarchical form consisting of ~2- to 10-µm micropores partitioned by a nanoporous phase (Fig. 1B and fig. S4), P(VdF-HFP) exhibits high $\bar{R}_{solar}$ and $\bar{\epsilon}_{LWIR}$. Pore-size measurements indicate that the pore sizes are bimodally distributed, with broad distributions centered at ~0.2 and ~5.5 µm for the nano- and micropores, respectively (Fig. 2C) (*4*). As corroborated by finite-difference time-domain simulations (*4*), the abundant micropores with sizes ~5 µm efficiently scatter sunlight of all wavelengths (Fig. 2D). This is further enhanced by the nanopores with sizes ~50 to 500 nm, which strongly scatter shorter, visible wavelengths (Fig. 2D). The simulations are also experimentally substantiated by diffuse transmission characterizations, which yield a photon mean free path (l_f) of ~6 µm for the blue wavelengths and ~10 µm for the NIR wavelengths (fig. S3). In the absence of any intrinsic absorption,

[1]Department of Applied Physics and Applied Mathematics, Columbia University, New York, NY 10027, USA. [2]Department of Mechanical Engineering, Columbia University, New York, NY 10027, USA. [3]Advanced Photon Source, Argonne National Laboratory, Lemont, IL 60439, USA. [4]National Synchrotron Light Source II, Brookhaven National Laboratory, Upton, NY 11973, USA.
*Corresponding author. Email: yy2664@columbia.edu (Y.Y.); ny2214@columbia.edu (N.Y.)

this results in a high optical backscattering of sunlight and thus a matte, white appearance. Furthermore, the unoriented pores result in a high, diffuse $\bar{R}_{solar}(\theta)$ regardless of the angle of incidence (Fig. 1E). In the thermal wavelengths, the emittance is likely enhanced across the LWIR window by the broadening of the extinction peaks (Fig. 2B) due to impurities (e.g., moisture), polymer chain deformation, and amorphousness in the nanoporous polymer (20–22). We attribute the high $\bar{\epsilon}_{LWIR}(\theta)$ for a wide, angular range (Fig. 1F) to the open, porous surface (Fig. 1B) and the effective medium behavior of the nanoporous P(VdF-HFP)$_{HP}$ coating at large wavelengths (4). A combination of these two features provides a gradual refractive index transition across polymer-air boundaries. Therefore, emitted radiation is not hindered at the surface and $\bar{\epsilon}_{LWIR}(\theta)$ is high regardless of the angle (Fig. 2, E and F).

The high $\bar{R}_{solar}$ and $\bar{\epsilon}_{LWIR}$ allow P(VdF-HFP)$_{HP}$ coatings to achieve exceptional daytime subambient cooling under widely different skies of Phoenix (USA), New York (USA), and Chattogram (Bangladesh) (Fig. 3). For instance, under a peak solar intensity I_{solar} of ~890 W m^{-2} and a clear sky with low humidity in Phoenix, P(VdF-HFP)$_{HP}$ coatings without any convection shields achieved a subambient temperature drop (ΔT) of ~6°C. Promisingly, ΔT ~3°C was also observed in Chattogram, where fog and haze impeded radiative heat loss into the sky. P(VdF-HFP)$_{HP}$ coatings also attained exceptional cooling powers ($P_{cooling}$) (4) of 96 and 83 W m^{-2} in Phoenix and New York, respectively. The values are consistent with theoretical calculations (table S1) and indicate P(VdF-HFP)$_{HP}$'s potential to reduce air-conditioning costs of buildings. We cannot directly compare the performance to earlier results, as $P_{cooling}$ depends heavily on experimental design, geography, and meteorological variables (table S2) (23–25). Nevertheless, the high performance without convection shields in different climates indicate P(VdF-HFP)$_{HP}$'s PDRC capability is better than or on par with high-performance PDRC results in the literature (7, 9, 10).

The excellent optical performance of P(VdF-HFP)$_{HP}$ is complemented by a paint-like applicability, which is crucial for direct application on structures. We can paint, dip-coat, or spray P(VdF-HFP)$_{HP}$ onto diverse substrates like metal, plastics, and wood (Fig. 4, A to C). Furthermore, P(VdF-HFP)$_{HP}$ can also be made into strong, recyclable sheets (Fig. 4D and figs. S12 to S13). We also conducted accelerated thermal aging and moisture testing that showed the durability of the coatings and sheets (table S3). P(VdF-HFP) is intrinsically resistant to weathering, fouling, and UV radiation (21, 26). When made porous, it hydrophobically repels waterborne dirt (fig. S14). During accelerated aging and monthlong outdoor exposure tests, these properties enabled P(VdF-HFP)$_{HP}$ to retain its optical performance at near-pristine levels (table S3 and fig. S15). For instance, a monthlong outdoor exposure in New York City only changed $\bar{R}_{solar}/\bar{\epsilon}_{LWIR}$ from 0.94/0.93 to 0.93/0.93.

An often-unstated but important practical requirement for PDRC coatings is compatibility with colors. To minimize solar heating, colored PDRC coatings should maximize the reflection of NIR-to-SWIR wavelengths (0.7 to 2.5 µm), which contain ~51% of solar energy but are invisible to the human eye. However, paints typically have low reflectances ($\bar{R}_{NIR-SWIR}$) in the NIR-to-SWIR wavelengths (fig. S10) (13, 27). By contrast, porous P(VdF-HFP)$_{HP}$ coatings containing blue, yellow, and black dyes and with thickness ~350 µm efficiently backscatter sunlight not absorbed by the dyes to yield correspondingly colored coatings with high $\bar{R}_{NIR-SWIR}$ of 0.73, 0.89, and 0.62, respectively (Fig. 4, E and F). These values were measured with black substrates but exceed reflectances of thin films (~25 µm) of similarly colored "IR-reflective" pigments on reflective substrates (Fig. 4, F and G) and of the same pigments on black substrates by a large margin (27, 28). Dyed P(VdF-HFP)$_{HP}$ coatings may thus address the long-standing problem of achieving PDRC with colored coatings, greatly widening their scope of use.

The phase inversion–based technique, shown here for P(VdF-HFP)$_{HP}$, is compatible with a wide variety of polymers. The method thus allows optically suitable polymers to be easily structured into PDRC coatings with other potential benefits. For instance, poly(methyl methacrylate) yields glossy coatings, ethyl cellulose provides biocompatibility and enables use of eco-friendly solvents, and polystyrene enables operation at temperatures >200°C (fig. S16). The diverse possibilities makes
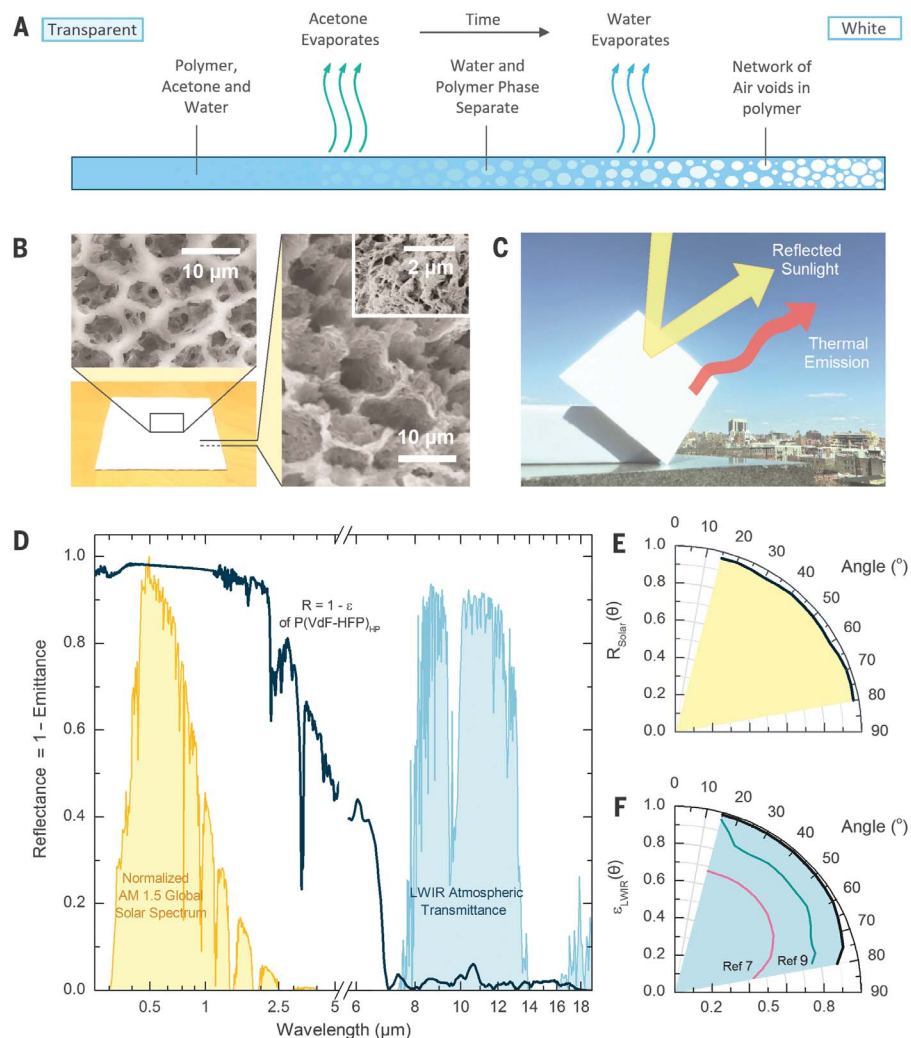

Fig. 1. The formation and optical properties of P(VdF-HFP)$_{HP}$ (**A**) Schematic of the phase inversion process, showing the formation of a hierarchically porous polymer coating from a solution of acetone (solvent), water (nonsolvent), and P(VdF-HFP) (polymer). (**B**) Micrographs showing top and cross-section views of P(VdF-HFP)$_{HP}$ Inset shows the nanoporous features. (**C**) Photograph superimposed with schematics to show that high $\bar{R}_{solar}$ and $\bar{\epsilon}_{LWIR}$ enable a net radiative loss and PDRC. (**D**) Spectral reflectance [$R(\lambda) = 1 - \epsilon(\lambda)$] of a 300-µm-thick P(VdF-HFP)$_{HP}$ coating presented against normalized ASTM G173 Global solar spectrum and the LWIR atmospheric transparency window. $\bar{R}_{solar}$ (0.96) and $\bar{\epsilon}_{LWIR}$ (0.97) are exceptionally high, especially given that they are achieved on a black selective solar absorber (fig. S2) (29). (**E**) P(VdF-HFP)$_{HP}$'s high $\bar{R}_{solar}(\theta)$ and (**F**) $\bar{\epsilon}_{LWIR}(\theta)$ across angles result in excellent hemispherical $\bar{R}_{solar}$ and $\bar{\epsilon}_{LWIR}$.
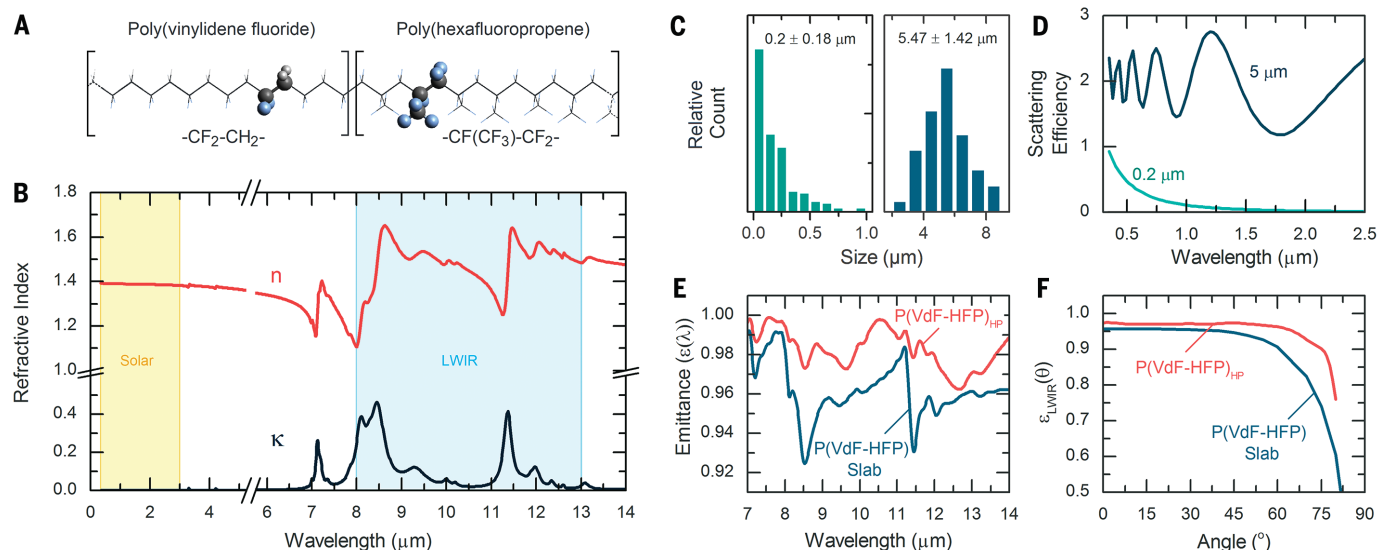
Fig. 2. The optical properties of P(VdF-HFP)_HP. (**A**) A wireframe showing the structure of P(VdF-HFP), with the VdF and HFP repeating units shown. (**B**) Experimental complex spectral refractive index ($n + i\kappa$) of P(VdF-HFP), showing negligible absorptivity in the solar, and high emissivity in the LWIR, wavelengths. The peaks in κ correspond to the vibrational modes of different molecular components (e.g., CF_3, CF_2, CF, C-C, CH_2, C-H, and carbon backbone) (17–19). (**C**) Size distributions of nano- and micropores in P(VdF-HFP)_HP showing number-weighted mean pore sizes of ~0.2 μm for nanopores and ~5.5 μm for micropores. (**D**) Simulated scattering cross-section spectra of circular micro- and nanovoids in P(VdF-HFP)_HP. Voids of different sizes collectively scatter all solar wavelengths, resulting in a high $\bar{R}_{solar}$. (**E**) Spectral LWIR emittance and (**F**) $\bar{\epsilon}_{LWIR}(\theta)$ of P(VdF-HFP)_HP compared to a solid P(VdF-HFP) slab of the same volume. As evident, the former has a higher spectral and angular emittance. Further details are provided in the supplementary materials (4).
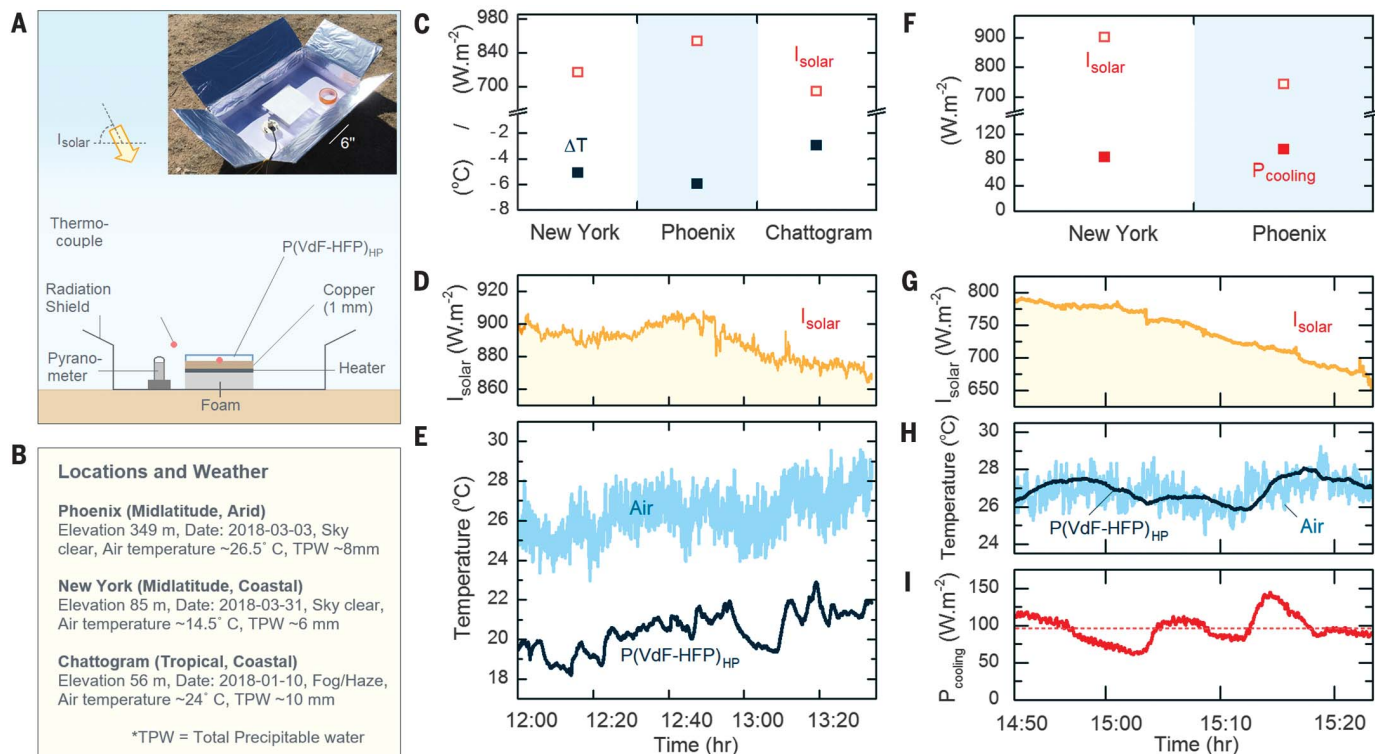
Fig. 3. Passive daytime radiative cooling performance of P(VdF-HFP)_HP. (**A**) Schematic of the setup for testing performance under sunlight. (**B**) Topographic and meteorological information of the test locations. (**C**) Average solar intensity (I_{solar}) and subambient temperature drops (ΔT) of P(VdF-HFP)_HP coatings in New York, Phoenix, and Chattogram. (**D**) Detailed I_{solar} and (**E**) temperature data of the result for Phoenix in (C). (**F**) I_{solar} and cooling powers ($P_{cooling}$) of P(VdF-HFP)_HP coatings measured in New York and Phoenix. (**G**) Detailed I_{solar}, (**H**) temperature tracking, and (**I**) $P_{cooling}$ data of the result for Phoenix in (F). Dotted line in (I) indicates average $P_{cooling}$ over the duration of the experiment. Additional information is provided in the supplementary materials (4).
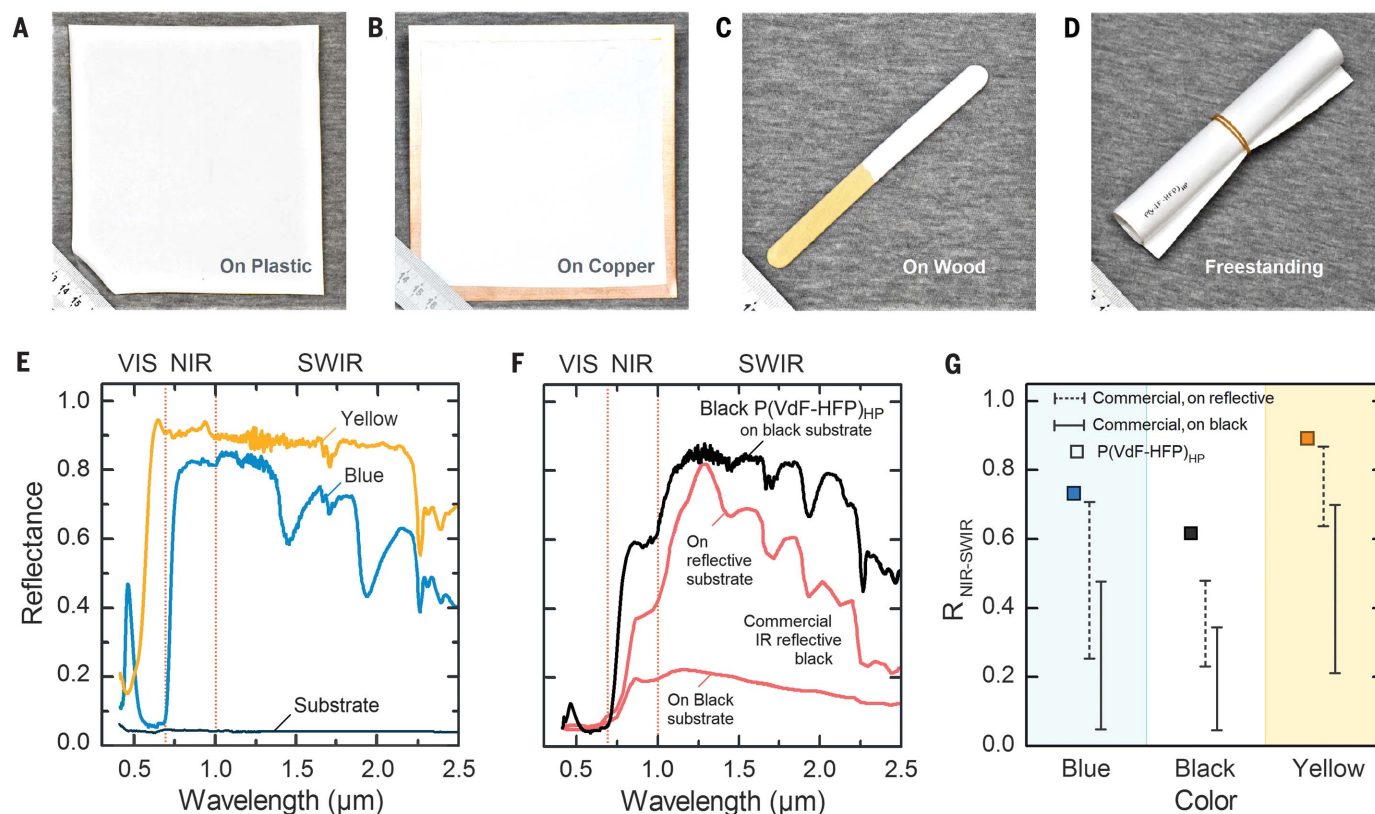
Fig. 4. Versatility of P(VdF-HFP)$_{HP}$ coatings. P(VdF-HFP)$_{HP}$ can be (**A**) painted onto plastics, (**B**) spray-coated on copper, (**C**) dip-coated on wood, and (**D**) made into strong, flexible, and freestanding sheets for tarpaulin-like designs. (**E**) Spectral reflectances of ~350-μm-thick blue and yellow P(VdF-HFP)$_{HP}$ coatings and (**F**) of a black P(VdF-HFP)$_{HP}$ coating compared to a commercial black pigment on reflective and black substrates. (**G**) Despite being on black substrates, their $\bar{R}_{NIR-SWIR}$ surpasses those of similarly colored "IR-reflective" pigments (~25-μm-thick films) on both black and reflective substrates.

the phase inversion–based technique a viable pathway for making both generic and specialized PDRC coatings.

REFERENCES AND NOTES

1. M. Burke, S. M. Hsiang, E. Miguel, *Nature* **527**, 235–239 (2015).
2. World Bank, (2017). *Access to Electricity*. Retrieved from https://data.worldbank.org/indicator/EG.ELC.ACCS.RU.ZS.
3. United States Environment Protection Agency, (2018). *Phaseout of Ozone-Depleting Substances (ODS)*. Retrieved from https://www.epa.gov/ods-phaseout.
4. Materials and methods are available in the supplementary materials.
5. T. S. Eriksson, S. J. Jiang, C. G. Granqvist, *Sol. Energy Mater.* **12**, 319–325 (1985).
6. C. G. Granqvist, A. Hjortsberg, *Appl. Phys. Lett.* **36**, 139–141 (1980).
7. A. P. Raman, M. A. Anoma, L. Zhu, E. Rephaeli, S. Fan, *Nature* **515**, 540–544 (2014).
8. A. R. Gentle, G. B. Smith, *Nano Lett.* **10**, 373–379 (2010).
9. A. R. Gentle, G. B. Smith, *Adv. Sci.* **2**, 1500119 (2015).
10. Y. Zhai *et al.*, *Science* **355**, 1062–1066 (2017).
11. N. Yu, J. Mandal, A. C. Overvig, N. N. Shi, Patent WO 2016205717A1 (2016).
12. C. S. Wojtysiak, J. W. Butler, Patent PCT/AU02/00695 (2009).
13. J. Song *et al.*, *Sol. Energy Mater. Sol. Cells* **130**, 42–50 (2014).
14. G. T. J. Bentley, *Introduction to Paint Chemistry* (Springer Science, Bristol, UK, ed. 4, 1998).
15. Cool Roof Rating Council, *Rated Products Directory*. Retrieved from https://coolroofs.org/directory.
16. A. Al-Kattan *et al.*, *Environ. Sci. Technol.* **48**, 6710–6718 (2014).
17. Y. Bormashenko, R. Pogreb, O. Stanevsky, E. Bormashenko, *Polym. Test.* **23**, 791–796 (2004).
18. M. Kobayashi, K. Tashiro, H. Tadokoro, *Macromolecules* **8**, 158–171 (1975).
19. L. N. Sim, S. R. Majid, A. K. Arof, *Vib. Spectrosc.* **58**, 57–66 (2012).
20. H. Hagemann, R. G. Snyder, A. J. Peacock, L. Mandelkern, *Macromolecules* **22**, 3600–3606 (1989).
21. Arkema (2017). *KYNAR® & KYNAR FLEX® PVDF Performance Characteristics and Data*. Retrieved from www.extremematerials-arkema.com/en/product-families/kynar-pvdf-family/download-performance-characteristics-data-brochure.
22. R. S. Bretzlaff, R. P. Wool, *Macromolecules* **16**, 1907–1917 (1983).
23. T. S. Eriksson, C. G. Granqvist, *Appl. Opt.* **21**, 4381–4388 (1982).
24. A. W. Harrison, M. R. Walton, *Sol. Energy* **20**, 185–188 (1978).
25. C. J. Chen, in *Physics of Solar Energy* (Wiley, 2011), pp. 77–104.
26. Arkema (2008). *New fluoropolymer latex technology for cool materials solutions across an expanded color space*. Retrieved from http://coolcolors.lbl.gov/assets/docs/PAC-2008-03-06/Arkema-slides.pdf.
27. BASF, (2017) *Ultra-cool - The new heat reflective coatings from BASF*. Retrieved from www2.basf.us/pdfs/ULTRA-Cool.pdf.
28. R. Levinson, P. Berdahl, H. Akbari, *Sol. Energy Mater. Sol. Cells* **89**, 351–389 (2005).
29. J. Mandal *et al.*, *Adv. Mater.* **29**, 201702156 (2017).

Science

Hierarchically porous polymer coatings for highly efficient passive daytime radiative cooling

Jyotirmoy Mandal, Yanke Fu, Adam C. Overvig, Mingxin Jia, Kerui Sun, Norman N. Shi, Hua Zhou, Xianghui Xiao, Nanfang Yu and Yuan Yang

Painting on the cool

Passive radiative cooling materials emit heat. They can reduce the need for air conditioning by providing daytime cooling but are often challenging to apply to rooftops and other building surfaces. Mandal *et al.* fabricated porous poly(vinylidene fluoride-co-hexafluoropropene) to create an excellent radiative cooling material. Better yet, the polymer is easy to paint or spray onto a wide range of surfaces, has good durability, and can even be dyed. This makes it a promising candidate for widespread use as a high-performance passive radiative cooling material.
Science, this issue p. 315

ARTICLE TOOLS	http://science.sciencemag.org/content/362/6412/315
SUPPLEMENTARY MATERIALS	http://science.sciencemag.org/content/suppl/2018/09/26/science.aat9513.DC1
REFERENCES	This article cites 21 articles, 1 of which you can access for free http://science.sciencemag.org/content/362/6412/315#BIBL
PERMISSIONS	http://www.sciencemag.org/help/reprints-and-permissions

Use of this article is subject to the Terms of Service